SUPPLEMENTARY APPENDIX

Histone modifier gene mutations in peripheral T-cell lymphoma not otherwise specified

Meng-Meng Ji,[1] Yao-Hui Huang,[1] Jin-Yan Huang,[1] Zhao-Fu Wang,[2] Di Fu,[1] Han Liu,[1] Feng Liu,[1] Christophe Leboeuf,[3,4] Li Wang,[1,3] Jing Ye,[3] Yi-Ming Lu,[3] Anne Janin,[3,4] Shu Cheng[1] and Wei-Li Zhao[1,3]

[1]State Key Laboratory of Medical Genomics, Shanghai Institute of Hematology; Shanghai Rui Jin Hospital, Shanghai Jiao Tong University School of Medicine, China; [2]Department of Pathology, Shanghai Rui Jin Hospital; Shanghai Jiao Tong University School of Medicine, China; [3]Pôle de Recherches Sino-Français en Science du Vivant et Génomique, Laboratory of Molecular Pathology, Shanghai, China and [4]U1165 Inserm/Université Paris 7, Hôpital Saint Louis, Paris, France

**M-MJ, Y-HH, J-YH and Z-FW contributed equally to this work.*

 doi:10.3324/haematol.2017.182444

Received: October 13, 2017.

Accepted: January 3, 2018.

Pre-published: January 5, 2018.

Correspondence: zhao.weili@yahoo.com or orenge@medmail.com.cn

Supplemental Information

Histone modifier gene mutations in peripheral T-cell lymphoma not otherwise specified

Meng-Meng Ji[1†], Yao-Hui Huang[1†], Jin-Yan Huang[1†], Zhao-Fu Wang[2†], Di Fu[1], Han Liu[1], Feng Liu[1], Christophe Leboeuf[3,4], Li Wang[1,3], Jing Ye[3], Yi-Ming Lu[3], Anne Janin[3,4], Shu Cheng[1*], and Wei-Li Zhao[1,3*]

[†] These authors equally contributed to this work.

[1] State Key Laboratory of Medical Genomics; Shanghai Institute of Hematology; Shanghai Rui Jin Hospital; Shanghai Jiao Tong University School of Medicine; Shanghai, China;

[2] Department of Pathology, Shanghai Rui Jin Hospital; Shanghai Jiao Tong University School of Medicine; Shanghai, China;

[3] Pôle de Recherches Sino-Français en Science du Vivant et Génomique; Laboratory of Molecular Pathology; Shanghai, China;

[4] U1165 Inserm/Université Paris 7; Hôpital Saint Louis, Pairs, France

*** Corresponding Author:**

Wei-Li Zhao, Email: zhao.weili@yahoo.com, Shu Cheng, Email: orenge@medmail.com.cn, State Key Laboratory of Medical Genomics, Shanghai Institute of Hematology, Shanghai Rui Jin Hospital, 197 Rui Jin Er Road, Shanghai 200025, China. Tel: 0086-21-64370045, Fax: 0086-21-64743206.

Supplementary methods

DNA preparation

For frozen samples, genomic DNA was extracted with a DNeasy Blood and Tissue Mini Kit (Qiagen). For FFPE samples, genomic DNA was extracted with a QIAamp DNA FFPE Tissue Kit (Qiagen), according to the manufacturer's instructions.

Western blot

Cells were lysed in 200μl of lysis buffer (0.5M Tris-HCl, pH 6.8, 2mM EDTA, 10% glycerol, 2% SDS and 5% β-mercaptoethanol). Protein extracts (20μg) were electrophoresed on 10% SDS polyacrylamide gels and transferred to nitrocellulose membranes. Membranes were blocked with 5% nonfat dried milk in Tris-buffered saline (CWBIO, CW0042) and incubated for 2h at room temperature with the appropriate primary antibody, followed by a horseradish peroxidase-conjugated secondary antibody. The immunocomplexes were visualized using a chemiluminescence phototope-horseradish peroxidase kit (Cell Signaling Technologies, 7003). Anti-H3K4me1 (61633) and anti-H3K4me2 (39913) were from Active Motif. Anti-H3K4me3 (ab8580) and anti-H3K18Ac (ab1191) antibody were from Abcam. Horseradish

peroxidase-conjugated goat anti-mouse IgG (sc-2005) and goat anti-rabbit IgG (sc-2004) antibodies were from Santa Cruz Biotechnology. Histone (H3) (Proteintech, 17168-1-AP) was used to monitor equivalent protein loading.

Immunofluorescence and immunohistochemistry

Immunofluorescence assay was performed on acetone-fixed cells using an anti-H3K4me3 (Abcam, ab8580) antibody and an Alexa Fluor 488-conjugated goat anti-rabbit IgG (H+L) (ThermoFisher, A-11034) secondary antibody. Nuclei were counterstained with DAPI. Immunohistochemistry was performed on 5µm-paraffin sections with an indirect immunoperoxidase method using antibodies against H3K4me3 (Abcam, ab8580), H3K18ac (Abcam, ab1191) and p-ERK (Cell Signaling Technologies, 4370). Expression levels were scored semi-quantitatively based on the percentage of positive cells: +, <25%; ++, 25–49%; +++, 50–74%; ++++, 75–100%.

Isobolographic analysis

To determine the synergistic effect of chidamide combined with decitabine, the combination index (CI) method described by Chou[1] and Talalay and the Calcusyn software program (Biosoft,

Cambridge, UK) for automated analysis were performed. This method allows quantitative determination of drug interactions, where CI<1, =1, and >1 indicate synergism, additive effect, and antagonism, respectively. When the drugs were combined, the CI values were calculated for each experiment and for combination experiment at a fixed concentration ratio. When at least 80% of CI values for a combination were <1, the drug combination was considered to be synergistic.

mRNA-seq library preparation and sequencing analysis

Total RNA (1μg) was purified using Ribo-Zero rRNA Removal Kits (Illumina). RNA size, concentration, and integrity were verified using Agilent 2100 Bioanalyzer (Agilent). RNA libraries were constructed by using rRNA-depleted RNAs with TruSeq Stranded Total RNA Library Prep Kit (Illumina) according to the manufacturer's instructions. Libraries were controlled for quality and quantified using BioAnalyzer 2100 system (Agilent). 10pM libraries were denatured as single-stranded DNA molecules, captured on Illumina flow cells, amplified in situ as clusters and finally sequenced for 150 cycles on Illumina HiSeq Sequencer. Paired-end reads were harvested from Illumina HiSeq Sequencer, and were quality controlled by Q30. After 3' adaptor-trimming and low quality reads removing by cutadapt software (v1.9), the high quality trimmed reads were aligned to the reference genome (UCSC hg19) guided by the Ensembl GFF

gene annotation file with hisat2 software (v2.0.4). Then, cuffdiff software (part of cufflinks) was used to get the gene level FPKM as the expression profiles of mRNA, and fold change and p-value were calculated based on FPKM, differentially expressed mRNA were identified. Pathway enrichment and GSEA analysis were performed based on the differentially expressed mRNAs. The data is available on NCBI (Accession number GSE104280).

ChIP-seq library preparation and sequencing analysis

Chromatin immunoprecipitation was performed according to Wamstad et al [2]. The yield of ChIPed DNA was determined via Quant IT fluorescence assay (Life Technologies) and enrichment efficiencies of ChIP reactions were evaluated by qPCR. Illumina sequencing libraries were generated with NEBNext® Ultra™ DNA Library Prep Kit (New England Biolabs) following the manufacturer's manual. The library quality was determined by Agilent 2100 Bioanalyzer (Agilent), and subjected to high-throughput 150bp paired-end sequencing on Illumina Hiseq sequencer according to the manufacturer's protocol. Q30 was used to perform quality control on the raw sequencing data. Adaptor-trimming and low quality reads were removed by cutadapt (v1.9.1) software. High quality reads were aligned to human genome (UCSC hg19) using bowtie2

software (v2.2.4) with default parameters. Peak calling was performed with MACS software (v1.4.3). Differentially enriched regions were identified by diffReps software (v1.55.4). The enriched peaks were annotated with the latest UCSC RefSeq database to connect the peak information with the gene annotation. KEGG Pathway analysis was performed on the peak-associated genes or differentially enriched peak-associated genes. Enriched peaks were visualized on UCSC Genome Browser. The data is available on NCBI (Accession number GSE104289).

TUNEL assay

TUNEL assay was performed by in situ cell death detection kit (Roche) and detected DNA fragmentation by fluorescence microscopy.

Murine model

Nude mice (4 to 5 weeks old, Shanghai Laboratory Animal Center, Shanghai, China) were injected subcutaneously with 4×10^7 KMT2D-mutated (V5486M) Jurkat cells into the right flank. Treatments (10 mice per group) were started after the tumor became about 0.5×0.5cm in surface (day 0). The untreated group received RPMI1640, whereas the other three groups received twice

weekly for three weeks of chidamide (12.5 mg/kg) and/or decitabine (0.5 mg/kg), respectively. Tumor volumes were calculated as $0.5\times a(\text{length})\times b(\text{width})^2$. Animals were used according to the protocols approved by the Shanghai Rui Jin Hospital Animal Care and Use Committee.

Micro-PET-CT imaging

Mice were subjected to positron emission tomography-computed tomography (PET-CT) analysis after 21 days of treatment. PET-CT imaging was performed on an Inveon MM Platform (Siemens Preclinical Solutions) with 8.5cm transaxial and 5.7cm axial fields of view. 18F-fluorodeoxyglucose (0.1ml per injection with an activity of 10MBq) was injected to anesthetized mice through the tail vein. Mice were placed prone on the PET scanner bed 45 min later near the central field of view for scanning process in Inveon Acquisition Workplace 1.5.0.28. Ten-minute CT X-ray for attenuation correction was scanned with a power of 80kV and 500μA and an exposure time of 1100 ms before PET scan. Ten-minute static PET scans were then acquired, and images were reconstructed by an OSEM3D (three-dimensional ordered subsets expectation maximum) algorithm followed by MAP (maximization/maximum a posteriori) or FastMAP provided by Inveon Acquisition Workplace. The three-dimensional regions of interest were drawn over the heart guided by CT images and tracer uptake was measured using the

software of Inveon Research Workplace (IRW) 3.0. Individual quantification of the 18F-fluorodeoxyglucose uptake in each of them was calculated. Mean standardized uptake values were determined by dividing the relevant regions of interest concentration by the ratio of the injected activity to the body weight.

Reference

1. Chou TC. Theoretical basis, experimental design, and computerized simulation of synergism and antagonism in drug combination studies. Pharmacol Rev. 2006;58(3):621-681.

2. Wamstad JA, Alexander JM, Truty RM, et al. Dynamic and coordinated epigenetic regulation of developmental transitions in the cardiac lineage. Cell. 2012;151(1):206-220.

Supplemental Table 1. Mutation information of 125 patients with PTCL-NOS

Gene	Patient ID	Chromosome	Start*	End*	Reference Allele	Variant Allele	Amino Acid Change	Mutation Type
ARID1B	P20A	chr6	157150392	157150392	G	A	p.R525K	missense
ARID1B	P25A	chr6	157470024	157470024	C	T	p.R940C	missense
ARID1B	P19A	chr6	157528306	157528306	G	A	p.E2011K	missense
ARID1B	P22A	chr6	157528639	157528639	C	T	p.R2122C	missense
ARID1B	P109A	chr6	157528682	157528682	C	T	p.S2136L	missense
ARID2	P75A	chr12	46125020	46125020	G	A	p.W69_	nonsense
ARID2	P115A	chr12	46244926	46244926	T	C	p.L1007S	missense
CREBBP	P114	chr16	3778390	3778390	C	T	p.G2220S	missense
CREBBP	P7	chr16	3778390	3778390	C	T	p.G2220S	missense
CREBBP	P52	chr16	3778525	3778525	T	C	p.N2175D	missense
CREBBP	P66	chr16	3779814	3779814	C	T	p.W1745_	nonsense
CREBBP	P109	chr16	3807874	3807874	G	C	p.A1182G	missense
CREBBP	P52	chr16	3807914	3807914	G	A	p.R1169C	missense
CREBBP	P52	chr16	3860673	3860673	G	C	p.S302R	missense
DNMT3A	P1	chr2	2644	2644	C	T	p.R882H	missense
DNMT3A	P31	chr3	2644	2644	C	T	p.R882H	missense
DNMT3A	P81	chr2	2644	2644	C	T	p.R882H	missense
DNMT3A	P52	chr4	2645	2645	G	A	p.R882C	missense
EP300	P2	chr22	41547874	41547874	C	T	p.S952L	missense
EP300	P35	chr22	41547981	41547981	G	A	p.E988K	missense
EP300	P117	chr22	41558771	41558771	T	C	p.L1239P	missense
EP300	P127	chr22	41564805	41564805	T	C	p.V1369A	missense
EP300	P106	chr22	41564829	41564829	A	G	p.H1377R	missense
EP300	P39	chr22	41566521	41566521	G	A	p.W1466_	nonsense
EP300	P116	chr22	41568594	41568594	A	T	p.E1515V	missense
EP300	P116	chr22	41568605	41568605	G	T	p.E1519_	nonsense
EP300	P34	chr22	41572383	41572383	C	T	p.H1638Y	missense
EP300	P34	chr22	41572464	41572464	C	A	p.R1665S	missense

EP300	P38	chr22	41573584	41573584	C	G	p.P1957A	missense
EP300	P126	chr22	41573720	41573720	A	T	p.Q2002L	missense
KDM6A	P6	chrX	44922850	44922850	C	T	p.P571S	missense
KMT2A	P32	chr11	118378297	118378297	C	T	p.S3603F	missense
KMT2A	P4	chr11	118390680	118390680	C	T	p.A3777V	missense
KMT2A	P139	chr11	118392709	118392709	C	A/G	p.P3914H	missense
KMT2D	P109	chr12	49415845	49415845	C	T	p.R5501Q	missense
KMT2D	P26	chr12	49415883	49415883	T	A	p.L5488F	missense
KMT2D	P26	chr12	49415891	49415891	C	T	p.V5486M	missense
KMT2D	P21	chr12	49416381	49416381	C	T	p.E5444K	missense
KMT2D	P26	chr12	49416497	49416497	C	T	p.R5405H	missense
KMT2D	P115	chr12	49416600	49416600	C	T	p.E5371K	missense
KMT2D	P9	chr12	49420580	49420580	A	G	p.W5057R	missense
KMT2D	P54	chr12	49420606	49420606	C	T	p.R5048H	missense
KMT2D	P122	chr12	49426729	49426729	A	AGCT	p.Q3919fs	Frame_Shift
KMT2D	P97	chr12	49427347	49427347	C	T	p.R3714K	missense
KMT2D	P30	chr12	49427612	49427612	G	A	p.R3626W	missense
KMT2D	P7	chr12	49427983	49427983	C	T	p.R3536H	missense
KMT2D	P110	chr12	49427990	49427990	C	T	p.V3534I	missense
KMT2D	P33	chr12	49428067	49428067	C	T	p.R3508Q	missense
KMT2D	P34	chr12	49428067	49428067	C	T	p.R3508Q	missense
KMT2D	P110	chr12	49428077	49428077	C	T	p.A3505T	missense
KMT2D	P92	chr12	49431094	49431094	T	C	p.M3349V	missense
KMT2D	P125	chr12	49431305	49431305	T	TTGC	p.Q3278fs	Frame_Shift
KMT2D	Q1	chr12	49431688	49431688	G	A	p.A3151C	missense
KMT2D	P123	chr12	49431834	49431834	G	T	p.P3102H	missense
KMT2D	P101	chr12	49434507	49434507	G	A	p.P2349L	missense
KMT2D	P89	chr12	49434990	49434990	C	A	p.R2188L	missense
KMT2D	P37	chr12	49436348	49436348	A	G	p.S1955P	missense
KMT2D	P35	chr12	49438728	49438728	C	T	p.E1588K	missense
KMT2D	P35	chr12	49438741	49438741	C	A	p.Q1583H	missense
KMT2D	P26	chr12	49416546	49416546	G	A	p.R5389W	missense
KMT2D	P107	chr12	49426584	49426584	C	CTGT	p.Q3967fs	Frame_Shift

KMT2D	P113	chr12	49426599	49426599	C	CTGT	p.Q3962fs	Frame_Shift
KMT2D	P104	chr12	49426605	49426605	T	TTGTTGC	p.Q3961fs	Frame_Shift
KMT2D	P114	chr12	49426659	49426659	C	CTGT	p.Q3942fs	Frame_Shift
SETD2	P108	chr3	47108605	47108605	C	T	p.V2022I	missense
SETD2	P41	chr3	47108605	47108605	C	T	p.V2022I	missense
SETD2	P65	chr3	47125317	47125317	C	T	p.E1985K	missense
SETD2	P31	chr3	47147534	47147534	G	A	p.R1598_	nonsense
SETD2	P75	chr3	47147551	47147551	C	T	p.R1592Q	missense
SETD2	P46	chr3	47162057	47162057	G	A	p.L1357F	missense
TET1	P30A	chr10	70406580	70406580	C	T	p.T1365I	missense
TET1	P112A	chr10	70426934	70426934	C	T	p.R1532W	missense
TET1	P19A	chr10	70446140	70446140	C	T	p.R1694C	missense
TET1	P9A	chr10	70446263	70446263	G	A	p.E1735K	missense
TET1	P19A	chr10	70446318	70446318	G	A	p.R1753H	missense
TET2	P98	chr4	106155185	106155185	C	G	p.P29R	missense
TET2	P8	chr4	106155794	106155794	A	G	p.Q232R	missense
TET2	P111	chr4	106155887	106155887	A	G	p.E263G	missense
TET2	P74	chr4	106155911	106155911	C	G	p.S271_	nonsense
TET2	P28	chr4	106156747	106156747	C	T	p.R550_	nonsense
TET2	P46	chr4	106156747	106156747	C	T	p.R550_	nonsense
TET2	P112	chr4	106157956	106157956	G	A	p.T953R	missense
TET2	P36	chr4	106157971	106157971	C	T	p.Q958_	nonsense
TET2	P81	chr4	106164778	106164778	C	T	p.R1216_	nonsense
TET2	P77	chr4	106164913	106164913	C	G	p.R1261G	missense
TET2	P111	chr4	106190801	106190801	T	C	p.L1360P	missense
TET2	P55	chr4	106190866	106190866	C	T	p.H1382Y	missense
TET2	P116	chr4	106193925	106193925	A	T	p.T1463S	missense
TET2	P25	chr4	106157656	106157656	C	CT	p.L853fs	Frame_Shift
TET2	P31	chr4	106164780	106164780	A	AGCTGGC CACACCT GTGAG	p.A1217fs	Frame_Shift
TET2	P39	chr4	106197252	106197252	T	TG	p.V1862fs	Frame_Shift

Supplemental Table 2. Clinical characteristics of patients with PTCL-NOS (N=239)

Characteristics	Training Cohort	Validation Cohort		P value[1]	P value[2]
	(N=140)	CHOP-based (N=49)	Sequential (N=50)		
Gender					
Male	84/140 (60.0%)	33/49 (67.3%)	34/50 (68.0%)	0.276	1.000
Female	56/140 (40.0%)	16/49 (32.7%)	16/50 (32.0%)		
Age (years)					
≤60	81/140 (57.9%)	28/49 (57.1%)	29/50 (58.0%)	1.000	1.000
>60	59/140 (42.1%)	21/49 (42.9%)	21/50 (42.0%)		
Performance status (ECOG)					
0-1	101/140 (72.1%)	39/49 (79.6%)	40/50 (80.0%)	0.223	1.000
≥2	39/140 (27.9%)	10/49 (20.4%)	10/50 (20.0%)		
Lactic dehydrogenase					
Normal	58/140 (41.4%)	21/49 (42.9%)	22/50 (44.0%)	0.791	1.000
Elevated	82/140 (58.6%)	28/49 (57.1%)	28/50 (56.0%)		
Ann Arbor Stage					
I-II	43/140 (30.7%)	15/49 (30.6%)	17/50 (32.0%)	0.888	0.830
III-IV	97/140 (69.3%)	34/49 (69.4%)	33/50 (68.0%)		
Extranodal involvement					
0-1	104/140 (74.3%)	38/49 (77.6%)	39/50 (78.0%)	0.646	1.000
≥2	36/140 (25.7%)	11/49 (22.4%)	11/50 (22.0%)		
International prognostic index (IPI)					
Low risk	45/140 (32.1%)	13/49 (26.5%)	15/50 (30.0%)	0.487	0.686
Low/intermediate risk	31/140 (22.1%)	19/49 (38.8%)	18/50 (36.0%)		
Intermediate/high risk	40/140 (28.5%)	11/49 (22.4%)	11/50 (22.0%)		
High risk	24/140 (17.1%)	7/49 (14.3%)	6/50 (12.0%)		
Complete response					
Yes	61/140 (43.6%)	21/49 (42.9%)	23/50 (46.0%)	0.896	0.840
No	79/140 (56.4%)	28/49 (57.1%)	27/50 (54.0%)		
Histone modifier gene mutations					

Total	31/73 (42.5%)	7/26 (26.9%)	8/26 (30.7%)	0.136	1.000
KMT2D	18/73 (24.7%)	3/26 (11.5%)	4/26 (19.2%)		
SETD2	4/73 (5.5%)	1/26 (3.8%)	1/26 (3.8%)		
KMT2A	1/73 (1.4%)	1/26 (3.8%)	1/26 (3.8%)		
KDM6A	1/73 (1.4%)	0/26 (0%)	0/26 (0%)		
EP300	7/73 (9.6%)	1/26 (3.8%)	2/26 (7.7%)		
CREBBP	4/73 (5.5%)	1/26 (3.8%)	0/26 (0%)		
EZH2	0/73 (0%)	0/26 (0%)	0/26 (0%)		

P value[1] indicated difference between training cohort and validation cohort.

P value[2] indicated difference between arm A and arm B within validation cohort.

Supplemental Table 3. Features of patients with PTCL-NOS upon treatment of chidamide (N=16)

Sample ID	Gender	Age	IPI	Mutations
197	M	31	1	*KMT2D*
191	M	58	3	/
204	F	65	2	*KMT2D*
229	M	30	0	*CREBBP*
207	F	67	3	/
206	M	62	3	*KMT2D*
216	M	53	2	/
212	M	43	0	/
230	M	45	0	*KMT2D*
228	M	58	3	*EP300*
270	M	25	2	/
218	M	58	1	*EP300*
209	M	64	2	/
219	M	75	3	/
231	M	60	0	/
315	M	65	NA	/

Supplemental Figure 1. Schematic location and sequence alignment of *KMT2D/KMT2A* and *EP300/CREBBP* mutations in PTCL-NOS.

(a) Schematic location of *KMT2D/KMT2A* and *EP300/CREBBP* mutations.

(b) Sequence alignment of KMT2D/KMT2A and EP300/CREBBP protein across distinct species.

PHD, plant homeodomain, residues 134-320, 1378-1556, 5032-5138, and 1433-1624, 1871-1983, respectively; HMG, high-mobility group, residues 2021-2072; Undetermined domain, residues 2487-4658; FYRN, FY-rich, N-terminal, residues 5182-5232 and 2025-2071, respectively; FYRC, FY-rich, C-terminal, residues 5240-5327 and 3669-3752, respectively; SET, Su(var)3-9, Enhancer-of-zeste, Trithorax, residues 5397-5519 and 3825-3969, respectively. KIX, residues 566-646 and 587-667, respectively; Bromo, bromo cbp like, residues 1051-1158 and 1087-1194, respectively; HAT, histone acetylation protein, residues 1306-1612 and 1342-1649, respectively; ZZ, zinc finger, residues 1668-1708 and 1705-1745, respectively.

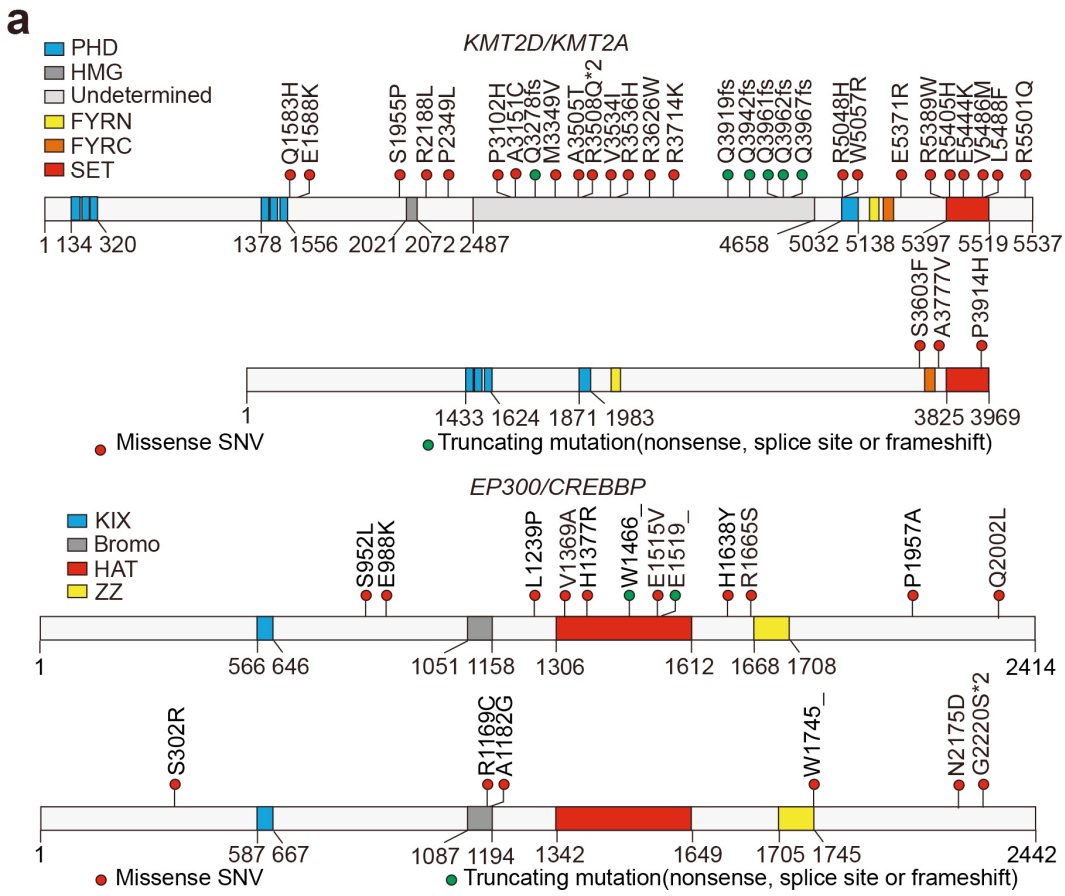
a
KMT2D/KMT2A
PHD
HMG
Undetermined
FYRN
FYRC
SET
Q1583H
E1588K
S1955P
R2188L
P2349L
P3102H
A3151C
Q3278fs
M3349V
A3505T
R3508Q*2
V3534I
R3536H
R3626W
R3714K
Q3919fs
Q3942fs
Q3961fs
Q3962fs
Q3967fs
R5048H
W5057R
E5371R
R5389W
R5405H
E5444K
V5486M
L5488F
R5501Q
1 134 320
1378 1556 2021 2072 2487
4658 5032 5138 5397 5519 5537
S3603F
A3777V
P3914H
1
1433 1624 1871 1983
3825 3969
Missense SNV
Truncating mutation(nonsense, splice site or frameshift)
EP300/CREBBP
KIX
Bromo
HAT
ZZ
S952L
E988K
L1239P
V1369A
H1377R
W1466_
E1515V
E1519_
H1638Y
R1665S
P1957A
Q2002L
1
566 646
1051 1158
1306
1612
1668 1708
2414
S302R
R1169C
A1182G
W1745_
N2175D
G2220S*2
1
587 667
1087 1194
1342
1649
1705 1745
2442
Missense SNV
Truncating mutation(nonsense, splice site or frameshift)

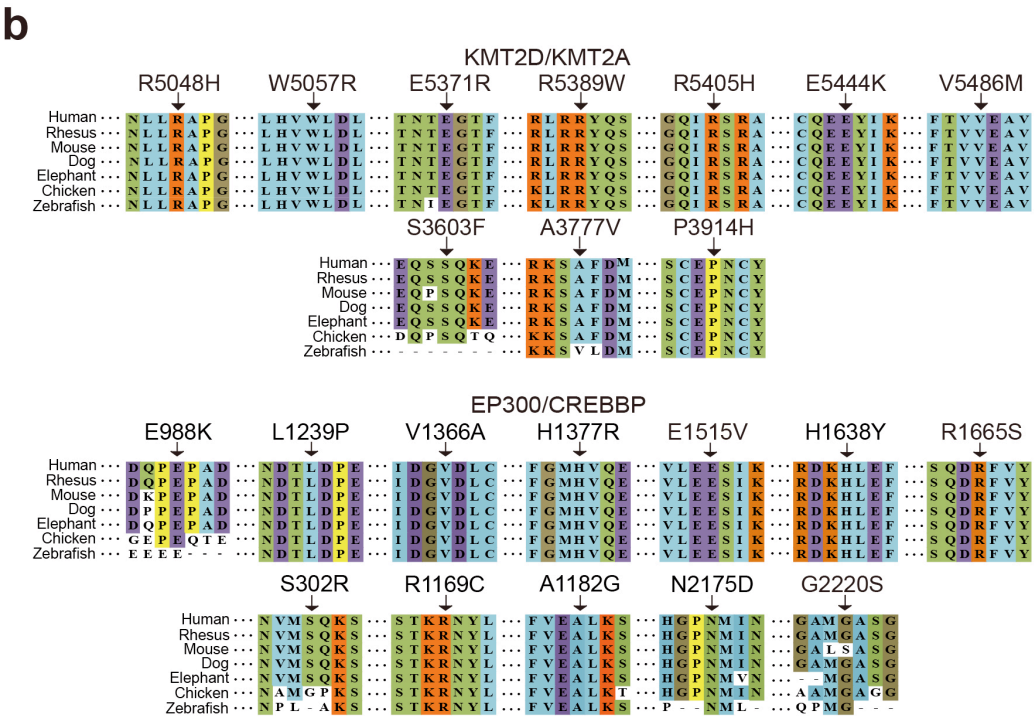
b
KMT2D/KMT2A
R5048H
W5057R
E5371R
R5389W
R5405H
E5444K
V5486M
Human
Rhesus
Mouse
Dog
Elephant
Chicken
Zebrafish
S3603F
A3777V
P3914H
EP300/CREBBP
E988K
L1239P
V1366A
H1377R
E1515V
H1638Y
R1665S
S302R
R1169C
A1182G
N2175D
G2220S

Supplemental Figure 2. Western blot of Jurkat cells transfected with wild-type (WT) KMT2D and KMT2D mutants (V5486M) upon treatment of different HDACI.